Integrated Optical Coherence Tomography and Optical Coherence Microscopy Imaging of Human Pathology

Citation: Lee, Hsiang-Chieh et al. "Integrated optical coherence tomography and optical coherence microscopy imaging of human pathology." Three-Dimensional and Multidimensional Microscopy: Image Acquisition and Processing XVII. Ed. Jose-Angel Conchello et al. San Francisco, California, USA: SPIE, 2010. 75700J-8. ©2010 COPYRIGHT SPIE--The International Society for Optical Engineering.

As Published: http://dx.doi.org/10.1117/12.843283

Publisher: SPIE

Persistent URL: http://hdl.handle.net/1721.1/58530

Version: Final published version: final published article, as it appeared in a journal, conference proceedings, or other formally published context

Integrated Optical Coherence Tomography and Optical Coherence Microscopy Imaging of Human Pathology

Hsiang-Chieh, Lee[1], Chao Zhou[1], Yihong Wang[2, 3], Aaron D. Aguirre[1, 4], Tsung-Han Tsai[1], David W. Cohen[2], James L. Connolly[2], James G. Fujimoto[1]

[1]Department of Electrical Engineering and Computer Science and Research Laboratory of Electronics, Massachusetts Institute of Technology, Cambridge, MA, USA
[2]Department of Pathology, Beth Israel Deaconess Medical Center, Harvard Medical School, Boston, MA, USA
[3]Department of Pathology, Montefiore Medical Center and Albert Einstein Medical School, Bronx, NY, USA
[4]Harvard-MIT Division of Health Sciences and Technology, Cambridge, MA, USA

ABSTRACT

Excisional biopsy is the current gold standard for disease diagnosis; however, it requires a relatively long processing time and it may also suffer from unacceptable false negative rates due to sampling errors. Optical coherence tomography (OCT) is a promising imaging technique that provide real-time, high resolution and three-dimensional (3D) images of tissue morphology. Optical coherence microscopy (OCM) is an extension of OCT, combining both the coherence gating and the confocal gating techniques. OCM imaging achieves cellular resolution with deeper imaging depth compared to confocal microscopy. An integrated OCT/OCM imaging system can provide co-registered multiscale imaging of tissue morphology. 3D-OCT provides architectural information with a large field of view and can be used to find regions of interest; while OCM provides high magnification to enable cellular imaging. The integrated OCT/OCM system has an axial resolution of <4um and transverse resolutions of 14um and <2um for OCT and OCM, respectively. In this study, a wide range of human pathologic specimens, including colon (58), thyroid (43), breast (34), and kidney (19), were imaged with OCT and OCM within 2 to 6 hours after excision. The images were compared with H & E histology to identify characteristic features useful for disease diagnosis. The feasibility of visualizing human pathology using integrated OCT/OCM was demonstrated in the pathology laboratory settings.

Keywords: Optical coherence tomography; optical coherence microscopy; human pathology

INTRODUCTION

Optical coherence tomography (OCT) is an emerging noninvasive biomedical imaging technique, which provides two- and three-dimensional imaging of tissue morphology using near infrared light [1]. The imaging principle of OCT is analogous to that of the ultrasound. OCT detects the echo time delay of the reflected light using a low coherence interferometer. The axial resolution of OCT is determined by the bandwidth of the light source. Utilizing femtosecond lasers or broadband superluminescent diodes (SLDs) as the light sources, OCT provides images with axial resolution of 2-3um in ophthalmology imaging and ~ 1um for other biomedical applications [2-5]. OCT enables noninvasive and high-resolution imaging of the specimens and has contributed significant improvement over the diagnosis of eye diseases. OCT imaging can reveal morphology features along with a variety of macular diseases, including age-related macular degeneration (AMD) and macular edema [2, 6, 7]. In addition, the nerve fiber layer thickness can be measured from the cross-sectional OCT images and can be used on the assessment of glaucoma diseases. In addition to ophthalmology application, OCT can also provide real time and high resolution images inside human bodies by integrating the endoscopic probe development [8, 9].

The recent development of optical coherence microscopy (OCM) has enabled OCT images with high transverse resolution of less than 2um. OCM reduces multiple scattering effect by combing high-sensitivity, coherence gated detection with standard confocal microscopy, leading to greater image contrast and imaging depth in highly scattering tissue [10-12]. The axial resolution of OCM is determined by both the coherence gate width provided by the light source, and the confocal gate width provided by the confocal pinhole. Although the imaging depth of OCM is better than that of standard confocal microscopy, the imaging area of OCM is relatively small compared with OCT. Therefore, an

Three-Dimensional and Multidimensional Microscopy: Image Acquisition and Processing XVII, edited by Jose-Angel Conchello, Carol J. Cogswell, Tony Wilson, Thomas G. Brown, Proc. of SPIE Vol. 7570, 75700J

integrated OCT/OCM system would be an ideal tool which can provide a multiscale imaging capability. The OCT engine in the integrated OCT/OCM system can provide images of tissue architectural features over a large field of view, while OCM engine can achieve cellular resolution imaging, but with a reduced field of view. *Ex vivo* imaging in the pathologic laboratory provides access to a wide range of pathological specimens. This also enables more controlled comparison to histology in order to validate new imaging modalities. In this study, we explore the feasibility of using integrated 3D-OCT and cellular resolution OCM imaging for the assessment of pathologies in various human tissues.

METHODS

A portable prototype integrated OCT/OCM system was developed in our group and was employed in the study. The system enables imaging of freshly excised pathological specimens in both the pathology laboratory and the endoscopic unit. A detail description of the integrated OCT/OCM system can be found in reference [13].

OCT/OCM images are generated using a compact broadband light source, which combines a Nd:Glass femtosecond laser and supercontinuum generation in a highly nonlinear fiber [14, 15]. The output of the broadband light source was connected to both the OCT and OCM engine with equal delivered power. The broadband light source enables both OCT and OCM images of axial resolution of less than 4um. Both OCT and OCM systems share the same fiber-optic scanning confocal microscope in the sample arm. Objectives with two difference magnification powers were mounted on the turret of the confocal microscope, which enabled rapid switching between the OCT and the OCM modalities. A fast two axis scanning galvanometer was implemented and enabled high-speed 3D-OCT images and the *en face* OCM images. In the OCT engine, the transverse resolution of the cross-sectional OCT images is 14um. A 3D-OCT dataset over the imaging volume of 3 x 1.5 x 1.3mm^3 (X x Y x Z), comprise 640 cross-sectional OCT images. Each cross-sectional OCT image is acquired at 1 frame/second. In the OCM engine, a broadband electro-optic modulator was deployed in the reference arm to provide a stable phase modulation of 1MHz. Novel dispersion compensation methods are developed to minimize the dispersion mismatch between the sample arm and the reference arm in the OCM engine [16]. OCM engine provides *en face* images with the field of view of ~400x400um^2 . The transverse resolution of the *en face* OCM image is 2um. A translation stage with scanning speed of 5 um/second was implemented to generate a 3D OCM dataset. The detection sensitivity is 98dB for both the OCT and OCM engines.

In addition to cross-sectional OCT images, e*n face* visualization of 3D-OCT dataset is realized. *En face* projected images at different imaging depths were constructed from 640 cross-sectional OCT images, demonstrating the larger field of view of OCT system (~1.5 x 3mm^2). A 10um averaging window was applied to suppress the speckle noise in the OCT images. The *en face* projected images are similar to conventional light microscopy images, which facilitates the examination of 3D-OCT dataset by pathologists.

The imaging protocol was approved by the institutional review board at the Beth Israel Deaconess Medical Center (BIDMC) and the Masssachusetts Institute of Technology (MIT). Specimens used in the current study were considered as discarded tissues and therefore informed consent was waived. Freshly excised human specimens were selected based on the presence of the pathology upon gross observation. Tissue selected (typically measured 1 x 1 x 0.5 cm^3) was preserved and transported to the imaging facility in RPMI medium 1640 (Invitrogen, Carlsbad, CA) as soon as possible. Integrated OCT/OCM imaging was generally performed within 2-6 hours after the excision. A thin cover slide was gently placed on the specimen to create a flat imaging surface and to reduce optical aberration. After imaging, the specimen was marked with Indian ink and fixed in 10% formalin before sending for histology processing. The specimens were sectioned along *en face* planes at different depths and stained with hematoxylin and eosin (H & E) to compare with *en face* OCT/OCM images.

RESULTS

Using the integrated OCT/OCM system, a wide range of human pathological specimens were imaged, including colon (58), thyroid (43), breast (34), and kidney (19). The imaging results were compared with histopathology and representative OCT/OCM images of human thyroid, breast and kidney are demonstrated in this proceeding.

Integrated OCT/OCM imaging of human thyroid

Thyroid cancer is the most common malignancy of the endocrine system [17]. There are approximately 37,200 new cases and 1,630 thyroid cancer deaths expected in the United Sates in 2009 [18]. Various methods are implemented to detect and screen for malignant thyroid nodules. To investigate the feasibility of using the integrated OCT/OCM system in differentiating benign and malignant thyroid nodules, *ex vivo* imaging of fresh excised thyroid tissue was performed [19]. Images of both normal and diseased thyroid specimens were compared with histological slides. Figure 1 shows OCT and OCM images of a normal human thyroid and the corresponding histology. From the *en face* projection OCT image shown in Figure 1 (a), well-organized round-to-oval thyroid follicles can be observed with size distribution from 50um to 500um in diameter. A single layer of epithelial cells lining the follicles can also be observed in high magnification OCM image as shown in Figure 1 (b), demonstrating the capability of cellular resolution imaging with OCM.

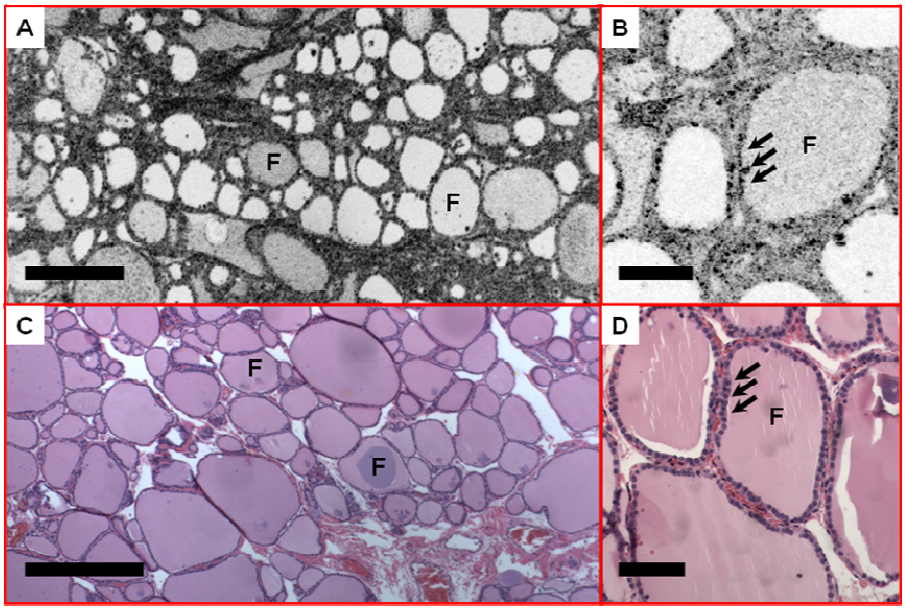

Figure 1. Normal thyroid demonstrates well-organized round-to-oval thyroid follicles (F). Colloid with various densities is observed under *en face* OCT (A) and OCM (B) obtained ~ 100um and 50um below the tissue surface, respectively, at different signal strengths. A single layer of epithelium (arrows), which are clearly seen in the OCM image (B) lines the follicles. (C) and (D) Corresponding H&E slides (4x and 20x, respectively). Scale bars, 500um in (A, C) and 100um in (B, D).

Figure 2 shows the integrated OCT/OCM images of a thyroid specimen with follicular variant papillary carcinoma. The tumor on the left side of Figure 2 (a) is clearly distinguished as densely packed micro-follicles (MF) and separated from the adjacent normal thyroid follicles on the lower right corner by a dense fibrous capsule (FI). OCM reveals the details of the microfollicles and normal follicles in Figure 2 (b) and (c), respectively. Although the resolution of OCM is not at the level of the cytology diagnosis, OCT and OCM can clearly differentiate microfollicular patterns and provide valuable information in assessing follicular variant of papillary carcinoma.

Integrated OCT/OCM imaging of human breast

Excluding skin cancer, breast cancer has been ranked as the second common cancer in women in the United States. There are an estimated 182,460 new cases of invasive breast cancer and 67,770 new cases of *in situ* breast cancer in the United States in 2009 [18]. Breast cancer also ranked as the second leading cause of death in women in 2009. Figure 3 (a) shows the characteristic pattern of a normal human breast. Fibrotic tissue, adipose tissue, blood vessels, and breast glands can be clearly identified in the *en face* OCT images. OCM image (Figure 3 (b)) shows the detailed structure of breast glands with higher magnification. Both the OCT and OCM images correlate well with corresponding histology shown in Figure 3 (c) and (d).

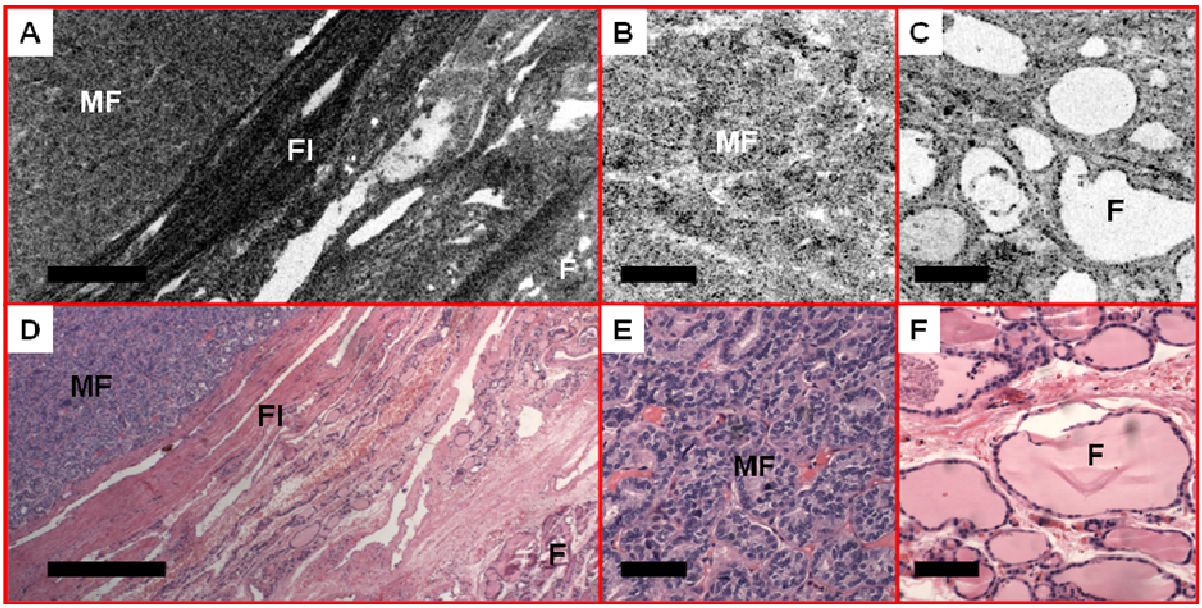

Figure 2. *En face* OCT (A) shows the tumor interface with normal thyroid tissue in papillary carcinoma, follicular variant. The tumor on the left side is clearly distinguished as densely packed micro follicles (MF) separated from the adjacent normal thyroid follicles (F) at the lower right corner by a dense fibrous (FI) capsule. Details of microfollicles and normal follicles are shown in the OCM images (B, C). The *en face* OCT and OCM images are obtained at depths of ~60um and 50um below the tissue surface, respectively. (D-F) Corresponding H&E slides (4x and 20x, respectively). Scale bars, 500um in (A,D) and 100um in (B,C,E, and F).

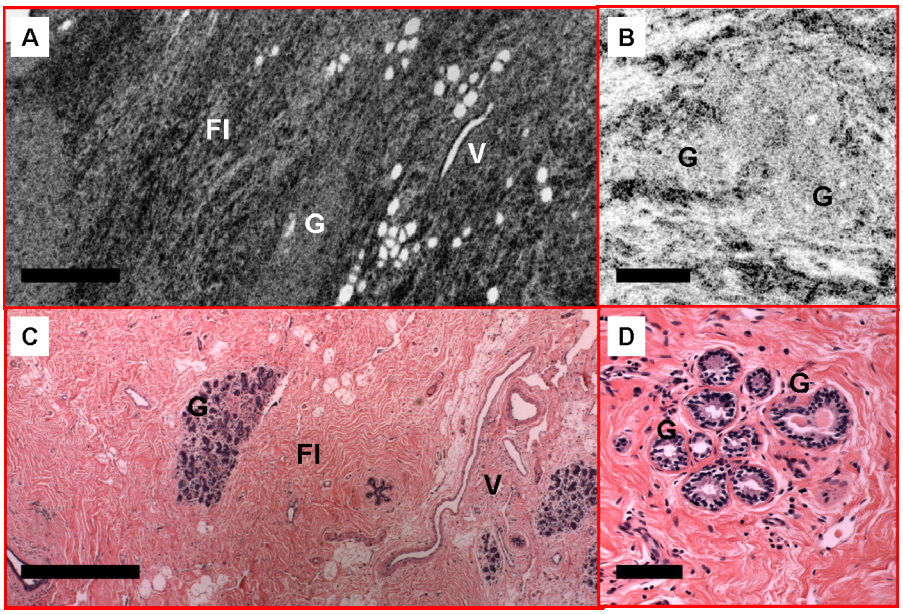

Figure 3. (A) *En face* OCT image of normal breast tissue shows fibrotic tissues "FI", blood vessels "V", and glands "G". (B) OCM reveals details of breast glands. (C, D) Corresponding histology. Scale bars are 500um in (A,C) and 100um in (B,D).

Integrated OCT/OCM imaging of human kidney

The most common type of kidney cancer is renal cell carcinoma (RCC), which accounts for approximately 85% renal parenchyma malignancies. In the United States, there are approximately over 50,000 new cases of kidney cancer diagnosed and 13,000 people died each year [18]. Among the new kidney cancers cases, 30,000 cases were diagnosed as RCC [20, 21]. Kidney tumor usually starts as a small mass without any pain, and becomes larger over time. There are various imaging methods for kidney cancer diagnosis including computed tomography (CT) scan, magnetic resonance imaging (MRI), ultrasound (US), and positron emission tomography (PET) [22, 23].

Figure 4 shows the representative images of normal kidney. Round spherical glomerulus structure (G) consisting of a convoluted network of capillaries can be observed in Figure 4 (a). Figure 4 (b) shows OCM image in the same imaging regions as Figure 4 (a), where the glomerulus structure and the surrounding tubules (T) can be visualized in more details. The average diameter of the glomerulus is around 150 to 200um. OCT and OCM images match well with the corresponding histology (Figure 4 (c) and (d)). The integrated OCT/OCM system can be used to distinguish changes in size and shape of the glomerulus, which has been shown to be an indicator of glomerulus diseases [24].

Figure 5 shows OCT/OCM images at the boundary between the cortex and the medulla of a normal human kidney. Figure 5 (a) shows an *en face* OCT projection generated from the 3D-OCT data set and it highlights the difference in tissue composition between cortex (Cx) and medulla (Md). Figure 5 (b) shows the OCM image over the cortex region and demonstrates the tubule structure (T). These results are consistent with the corresponding histology shown in Figure 5 (c) and (d).

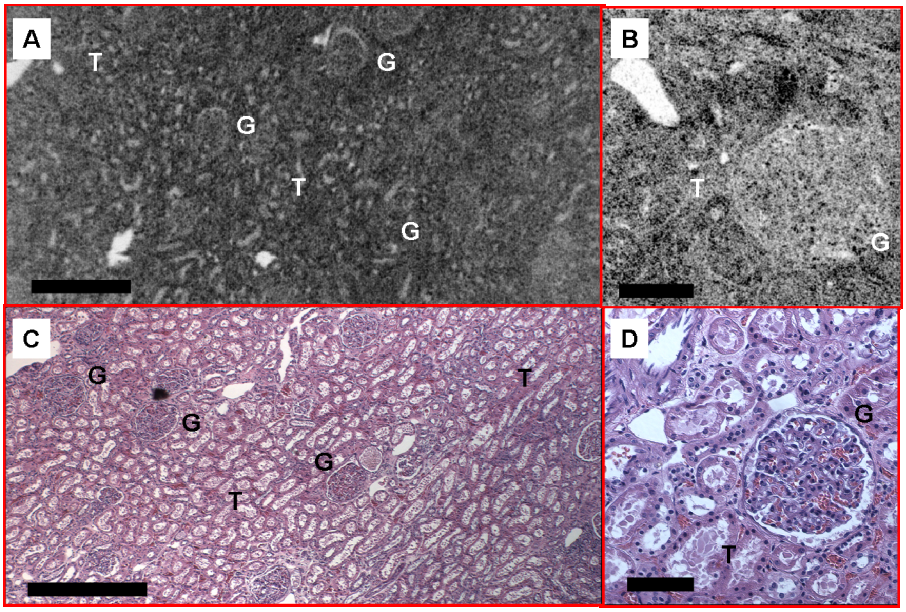

Figure 4. (A) *En face* OCT image of normal kidney, demonstrating the organized tissue structure composed of glomerulus (G) and a lot of tubules (T) surrounding each glomerulus. (B) OCM image reveals more detailed features of the glomerulus and also the surrounded tubules. (C,D) Corresponding histological images. Scale bars are 500um in (A,C) and 100um in (B,D).

DISCUSSIONS

The integrated OCT/OCM system provides multiscale images of the specimens and is potentially a complementary tool in the pathology examination. Compared with typical pathology examination using histology slides which require staining, OCT/OCM imaging utilizes the intrinsic light scattering properties of the specimens. Therefore, no fixation procedure is required for OCT/OCM imaging. Fresh excised specimens during the surgery or biopsy samples can be

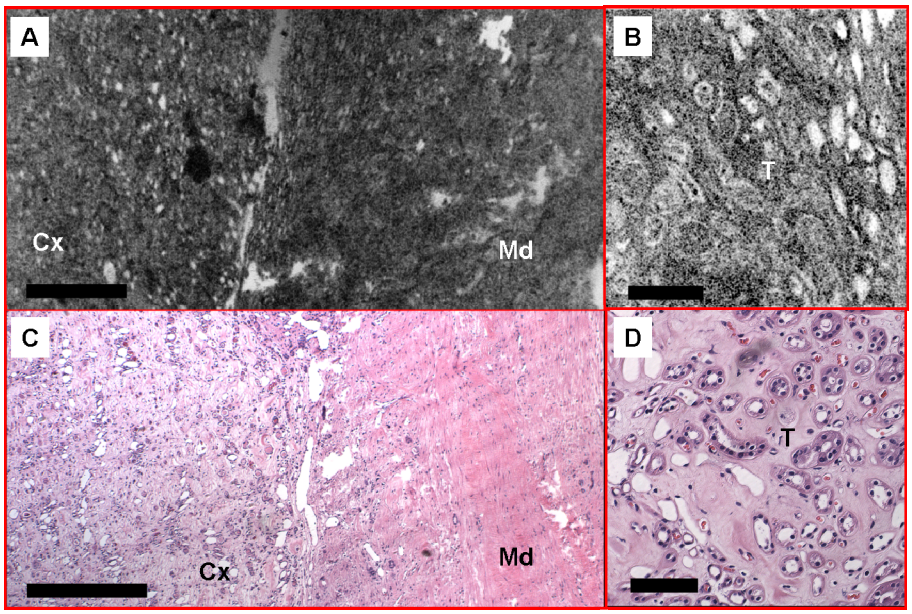

Figure 5. (A) *En face* OCT image of a normal human kidney over the regions between the cortex (Cx) and medulla (Md). (B) OCM image reveals the finer features of the tubules in the cortex regions. (C,D) Corresponding histologic images. Scale bars, 500um in (A,C) and 100um in (B,D).

imaged directly using the integrated OCT/OCM system, while the production of histology slides is time-consuming, leading to more efficient diagnosis processes.

3D-OCT provides large field of view images, enabling the gross observation of the specimens used to identify the regions of interest. The transverse resolution of the OCT images is sufficient in identifying the morphological features including the layer boundaries, cysts, blood vessels, and fibrotic structures. In addition, *en face* projected OCT images enable the examination of the specimens similar to conventional light microscopy. OCM images provide cellular information of the specimens and enable the examination of the specimens with finer resolution. Conventional light microscopy implements high NA objective to provide high rejection ratio of the unfocused light. However, utilizing the coherence detection scheme, OCM uses a relatively lower NA objective to improve the imaging depth while achieving cellular imaging resolution in the transverse dimension. The combination of high-sensitivity, confocal detection, and coherence-gated detection can extend the imaging depth in scattering media, thus increasing the imaging depth over standard confocal microscopy.

Therefore, integrated OCM/OCM system enables the visualization of both architectural characteristics and cellular features of the specimens at different resolution scales, and has the potential functioning as a complementary tool for pathologist in differentiating relevant features of different diseases. In glumerular diseases, especially the glomerulonephritis (GN), it has been demonstrated the glomerulus size will gradually increase in the early stage of the development of mesangial proliferative GN [24]. The integrated OCT/OCM system can be used to assess the size and distribution of the glomerulus in the kidney. In addition to the kidney diseases, OCT/OCM system can be implemented to assess the size and distribution of the follicle of human thyroid. In the future, OCT and OCM can be integrated with needle based imaging probes and coupled to fine needle aspiration to provide image guided biopsy. Therefore, the probability of sampling errors during FNA can be mitigated.

CONCLUSION

In summary, we have developed integrated OCT/OCM system and also demonstrated the OCT/OCM images of both normal and diseased human thyroid, breast and kidney. The integrated OCT/OCM system enables volumetric imaging of the specimens at different resolution scales. In addition, a seamless switching between OCT engine and OCM engine, in a way similar to conventional light microscopy facilitates the imaging procedures. Features in different normal and

pathological specimens are correlated with corresponding histology. The *ex vivo* OCT/OCM studies of the human pathologic specimens can serve as the reference for future *in vivo* examination of human pathology.

ACKNOWLEDGEMENTS

This work was supported by the NIH grants R01-CA75289-13 (J.G.F. and J.L.C.), Air Force Office of Scientific Research contract FA9550-07-1-0014 (J.G.F.), Medical Free Electron Laser Program contract FA9550-07-1-0101 (J.G.F.) and the MIT/CIMIT Medical Engineering Fellowship and Taiwan Merit Scholarship from the National Science Council of Taiwan (T.-H.T.).

REFERENCE

[1] D. Huang, E. A. Swanson, C. P. Lin, J. S. Schuman, W. G. Stinson, W. Chang, M. R. Hee, T. Flotte, K. Gregory, C. A. Puliafito, and J. G. Fujimoto, "Optical Coherence Tomography," *Science,* vol. 254, pp. 1178-1181, Nov 22 1991.

[2] W. Drexler, U. Morgner, R. K. Ghanta, F. X. Kärtner, J. S. Schuman, and J. G. Fujimoto, "Ultrahigh-resolution ophthalmic optical coherence tomography," *Nature Medicine,* vol. 7, pp. 502-507, Apr 2001.

[3] I. Hartl, X. D. Li, C. Chudoba, R. K. Hganta, T. H. Ko, J. G. Fujimoto, J. K. Ranka, and R. S. Windeler, "Ultrahigh-resolution optical coherence tomography using continuum generation in an air-silica microstructure optical fiber," *Optics Letters,* vol. 26, pp. 608-610, 2001/05/01 2001.

[4] J. G. Fujimoto, "Optical coherence tomography for ultrahigh resolution in vivo imaging," *Nature Biotechnology,* vol. 21, pp. 1361-1367, Nov 2003.

[5] W. Drexler, "Ultrahigh-resolution optical coherence tomography," *Journal of Biomedical Optics,* vol. 9, pp. 47-74, 2004/01/ 2004.

[6] W. Drexler, "Methodological advancements. Ultrahigh-resolution optical coherence tomography," *Ophthalmologe,* vol. 101, pp. 804-812, AUG 2004.

[7] W. Drexler, H. Sattmann, B. Hermann, T. H. Ko, M. Stur, A. Unterhuber, C. Scholda, O. Findl, M. Wirtitsch, J. G. Fujimoto, and A. F. Fercher, "Enhanced visualization of macular pathology with the use of ultrahigh-resolution optical coherence tomography," *Archives of Ophthalmology,* vol. 121, pp. 695-706, May 2003.

[8] X. D. Li, S. A. Boppart, J. Van Dam, H. Mashimo, M. Mutinga, W. Drexler, M. Klein, C. Pitris, M. L. Krinsky, M. E. Brezinski, and J. G. Fujimoto, "Optical coherence tomography: advanced technology for the endoscopic imaging of Barrett's esophagus," *Endoscopy,* vol. 32, pp. 921-30, Dec 2000.

[9] X. Li, C. Chudoba, T. Ko, C. Pitris, and J. G. Fujimoto, "Imaging needle for optical coherence tomography," *Optics Letters,* vol. 25, pp. 1520-2, 2000/10/15 2000.

[10] J. A. Izatt, M. R. Hee, E. A. Swanson, C. P. Lin, D. Huang, J. S. Schuman, C. A. Puliafito, and J. G. Fujimoto, "Micrometer-scale resolution imaging of the anterior eye in vivo with optical coherence tomography," *Archives of ophthalmology,* vol. 112, pp. 1584-9, Dec 1994.

[11] J. A. Izatt, M. D. Kulkarni, H.-W. Wang, K. Kobayashi, and M. V. Sivak, Jr., "Optical coherence tomography and microscopy in gastrointestinal tissues," *IEEE Journal of Selected Topics in Quantum Electronics,* vol. 2, pp. 1017-28, 1996/12/ 1996.

[12] M. Kempe, W. Rudolph, and E. Welsch, "Comparative study of confocal and heterodyne microscopy for imaging through scattering media," *Journal of the Optical Society of America a-Optics Image Science and Vision,* vol. 13, pp. 46-52, JAN 1996.

[13] A. D. Aguirre, P. R. Herz, Y. Chen, J. G. Fujimoto, W. Piyawattanametha, L. Fan, S. Hsu, M. Fujino, M. C. Wu, and D. Kopf, "Ultrahigh resolution OCT imaging with a two-dimensional MEMS scanning endoscope," San Jose, CA, United States, 2005, pp. 277-282.

[14] A. D. Aguirre, N. Nishizawa, J. G. Fujimoto, W. Seitz, M. Lederer, and D. Kopf, "Continuum generation in a novel photonic crystal fiber for ultrahigh resolution optical coherence tomography at 800 nm and 1300 nm," *Optics Express,* vol. 14, pp. 1145-1160, Feb 6 2006.

[15] S. Bourquin, A. D. Aguirre, I. Hartl, P. Hsiung, T. H. Ko, J. G. Fujimoto, T. A. Birks, W. J. Wadsworth, U. Bunting, and D. Kopf, "Ultrahigh resolution real time OCT imaging using a compact femtosecond Nd : Glass laser and nonlinear fiber," *Optics Express,* vol. 11, pp. 3290-3297, Dec 1 2003.

[16] A. D. Aguirre, J. Sawinksi, S.-W. Huang, C. Zhou, W. Denk, and J. G. Fujimoto, "High Speed Optical Coherence Microscopy with Autofocus Adjustment and a Miniaturized Endoscopic Imaging Probe," *Opt. Express,* vol. forthcoming, 2009.
[17] S. A. Hundahl, I. D. Fleming, A. M. Fremgen, and H. R. Menck, "A National Cancer Data Base Report on 53,856 Cases of Thyroid Carcinoma Treated in the US, 1985-1995," *Cancer,* vol. 83, pp. 2638-2648, Dec 15 1998.
[18] "Cancer Facts and Figures," American Cancer Society 2009 2009.
[19] C. Zhou, Y. H. Wang, A. D. Aguirre, T.-H. Tsai, J. L. Connolly, and J. G. Fujimoto, "Ex vivo Imaging of Human Thyroid Pathology Using Integrated Optical Coherence Tomography (OCT) and Optical Coherence Microscopy (OCM)," *Journal of Biomedical Optics,* vol. forthcoming, 2009.
[20] J. K. McLaughlin, L. Lipworth, and R. E. Tarone, "Epidemiologic aspects of renal cell carcinoma," *Seminars in Oncology,* vol. 33, pp. 527-533, Oct 2006.
[21] D. Pascual and A. Borque, "Epidemiology of kidney cancer," *Adv Urol,* p. 782381, 2008 (Epub 2008 Nov 2008.
[22] D. M. Bolton, P. Wong, and N. Lawrentschuk, "Renal cell carcinoma: imaging and therapy," *Current Opinion in Urology,* vol. 17, pp. 337-340, Sep 2007.
[23] K. Bouchelouche and P. Oehr, "Positron emission tomography and positron emission tomography/computerized tomography of urological malignancies: An update review," *Journal of Urology,* vol. 179, pp. 34-45, Jan 2008.
[24] S. Daimon and I. Koni, "Glomerular enlargement in the progression of mesangial proliferative glomerulonephritis," *Clinical Nephrology,* vol. 49, pp. 145-152, Mar 1998.